



4-25-2016

# Quantum Mechanical Interference in the Field Ionization of Rydberg Atoms

Jacob A. Hollingsworth

Ursinus College, jahollingsworth@ursinus.edu

Adviser: Thomas Carroll

Follow this and additional works at: [https://digitalcommons.ursinus.edu/physics\\_astro\\_hon](https://digitalcommons.ursinus.edu/physics_astro_hon)



Part of the [Atomic, Molecular and Optical Physics Commons](#)

**Click here to let us know how access to this document benefits you.**

## Recommended Citation

Hollingsworth, Jacob A., "Quantum Mechanical Interference in the Field Ionization of Rydberg Atoms" (2016). *Physics and Astronomy Honors Papers*. 1.

[https://digitalcommons.ursinus.edu/physics\\_astro\\_hon/1](https://digitalcommons.ursinus.edu/physics_astro_hon/1)

This Paper is brought to you for free and open access by the Student Research at Digital Commons @ Ursinus College. It has been accepted for inclusion in Physics and Astronomy Honors Papers by an authorized administrator of Digital Commons @ Ursinus College. For more information, please contact [aprock@ursinus.edu](mailto:aprock@ursinus.edu).

# QUANTUM MECHANICAL INTERFERENCE IN THE FIELD IONIZATION OF RYDBERG ATOMS

by

Jacob A. Hollingsworth

Department of Physics  
Ursinus College

April 27, 2015

Submitted to the Faculty of Ursinus College in fulfillment of  
the requirements for Honors in the Department of Physics.



Copyright © April 27, 2015 by Jacob A. Hollingsworth  
All rights reserved



# Abstract

Rydberg atoms are traditionally alkali metal atoms with their valence electron excited to a state of very large principle quantum number. They possess exaggerated properties, and are consequently an attractive area of study for physicists. An example of their exaggerated properties is seen in their response to the presence of an applied electric field. In this work, we study the energy distribution of Rydberg atoms when subjected to a dynamic electric field intended to ionize them.

We excite  $^{85}\text{Rb}$  atoms to a superposition of the  $46D_{5/2}$   $|m_j| = \frac{1}{2}$  and  $|m_j| = \frac{3}{2}$  states in the presence of a small initial electric field. After a delay time, the electric field is pulsed in order to ionize the atoms. The current produced by the ejected electrons is measured. Calculations and experimental data are presented which display interference effects between the amplitude from the components of the initial superposition.



## Acknowledgments

I would first like to thank my researcher advisor, Dr. Tom Carroll. Through the entirety of my undergraduate years, Tom has fostered my growth as a student researcher, as a physics major, and even beyond physics. His patience with me throughout this work has been unparalleled.

Additionally, I extend my gratitude to my fellow student, Michael Vennettilli, who has had significant contributions to this project at almost every step along the way. I would also like to thank Dr. Michael Noel and Rachel Feynman, our collaborators at Byrn Mawr College who work tirelessly to gather the experimental results for the work presented here.

Moreover, I also acknowledge and appreciate useful conversations with Dr. Adeel Ajaib, who, after I approached him with a question related to this work, developed an entire lecture on a topic he had last seen in graduate school in order to help me understand it. Finally, I would like to thank the National Science Foundation for providing the funding to make the following work possible.





# Contents

<b>List of Figures</b>	<b>ix</b>
<b>List of Tables</b>	<b>xi</b>
<b>1 Introduction</b>	<b>1</b>
1.1 Introduction . . . . .	1
1.2 The Experiment . . . . .	2
<b>2 The Stark Effect</b>	<b>5</b>
2.1 A Model . . . . .	5
2.2 Interpreting the Model . . . . .	7
<b>3 Computing Stark Maps</b>	<b>9</b>
3.1 The Hamiltonian of a Rydberg Atom . . . . .	9
3.2 Solving for the Matrix Elements . . . . .	11
3.3 A Sample Stark Map . . . . .	13
<b>4 Landau-Zener Theory</b>	<b>17</b>
4.1 Model of Population Dynamics at Avoided Crossings . . . . .	17
4.2 Solving the Landau-Zener Formula . . . . .	19
4.3 Evolving a State through Ionization . . . . .	22

<b>5</b>	<b>Alternative to Landau-Zener Theory</b>	<b>25</b>
5.1	The Algorithm . . . . .	25
5.2	Performing the Computation . . . . .	26
5.3	The Detector . . . . .	29
<b>6</b>	<b>Results</b>	<b>31</b>
6.1	Path to Ionization . . . . .	31
6.2	Ionization Currents . . . . .	32
6.3	Comparison of Oscillation Frequencies . . . . .	34
6.4	Discussion and Interpretation . . . . .	35
<b>7</b>	<b>Future Work</b>	<b>39</b>
7.1	Treatment of Ionization . . . . .	39
7.2	Casting to a Quantum Control Experiment . . . . .	41

# List of Figures

1.1	A timing diagram of the experiment considered in this thesis. . . . .	2
1.2	The excitation scheme used to excite to a superposition of Rydberg states. . . . .	4
2.1	A plot of the eigenenergies of our idealized model of interacting energy states. In red is the plot of our first eigenvalue, $E'_1$ . In black is the plot of our second eigenvalue, $E'_2$ . See (2.9) and (2.10). . . . .	7
3.1	The Stark map for $^{85}\text{Rb}$ around the $n = 43$ and $n = 44$ manifolds for the $ m_j  = \frac{1}{2}$ states. Shows the dependence of the observable energies on the applied electric field. . . . .	14
4.1	In black, solid lines, we have again plotted the eigenenergies of our idealized model of interacting energy states. In grey, dashed lines, we have plotted $\omega_1$ and $\omega_2$ . . . . .	22
5.1	The probability of a diabatic transfer occurring as the system is evolved through an avoided crossing for many different slew rates. The blue dots show the probability of transfer given by the Landau-Zener formula. The red dots show the probability of transfer given by the algorithm described in Section 5.1. . . . .	27
6.1	The amplitude tracked through the ionization ramp on a Stark map. The states in blue colors contain $ m_j  = \frac{1}{2}$ population, and those in red colors contain $ m_j  = \frac{3}{2}$ population. The black line towards the right of the figure gives the classical ionization limit, which approximates the location where ionization occurs. . . . .	32
6.2	Left: Experimental Ionization Current. Right: Simulated Ionization Current. A two peak distribution is observed. . . . .	33

6.3	Left: Size of the peaks in the ionization current observed in experiment. Right: Size of the peaks in the simulated ionization current. We see $\pi$ out of phase oscillations in both cases. . . . .	34
6.4	The low field Stark Map of the states in the initial superposition. The state in red is the 46d, $j = \frac{5}{2}$ , $ m_j  = \frac{1}{2}$ state. The state in blue is the 46d, $j = \frac{5}{2}$ , $ m_j  = \frac{3}{2}$ state. . . . .	35
6.5	Comparison of the frequency of the oscillations observed for different values of the initial electric field. Oscillations for an initial field of $F = .18975 \text{ V/cm}$ are shown in green, $F = .276 \text{ V/cm}$ are shown in purple, and $F = .3707 \text{ V/cm}$ are shown in blue. . . . .	36
6.6	A Mach-Zehnder interferometer. The possible paths the amplitude can take is indicated by the black lines. The blue, dashed lines represent 50/50 beam splitters. The red, solid lines represent perfect mirrors. . . . .	36

# List of Tables



# Chapter 1

## Introduction

### 1.1 Introduction

A Rydberg atom is an atom occupying an energy state of large principal quantum number  $n$ , also known as a Rydberg state. Rydberg atoms, which are traditionally alkali metals, possess valence electrons with a probability amplitude that primarily lies very far away from the nucleus of the atom. The remaining inner shell of electrons screens the charge of the nucleus, creating a positively charged ionic core. Thus, the behaviour of Rydberg atoms closely resembles the behaviour of the hydrogen atom. The large separation between ionic core and the valence electron also results in the atom possessing a large dipole moment. In turn, this leads to an extreme sensitivity to electric fields, as well as strong interactions with nearby Rydberg atoms [1].

Due to these properties, as well as their long coherence times, Rydberg atoms are an appealing quantum mechanical system for further study. In recent years, many interesting properties of Rydberg atoms have been uncovered. For instance, recent work has shown the existence of many-body effects, in which the interactions between atoms may not be treated as a collection of binary interactions between atoms [2, 3]. An example of this is the so-called Rydberg-blockade, in which the



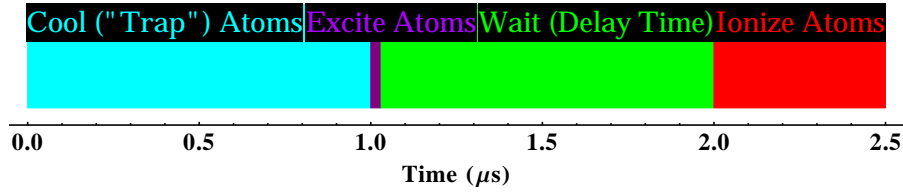


**Figure 1.1:** A timing diagram of the experiment considered in this thesis.

excitation of 1 atom to a Rydberg state prohibits the excitation of surrounding atoms [4]. Other groups have studied the behaviour of easily controllable, long range interactions between Rydberg atoms, known as dipole-dipole energy transfer [2,5,6]. Additionally, there has been significant work on the potential for Rydberg atoms to be used in the physical realization of a quantum computer [4,7–10].

## 1.2 The Experiment

We wish to probe the behaviour of Rydberg atoms in response to the presence of a changing electric field. To achieve this,  $^{85}\text{Rb}$  atoms are cooled to approximately  $100\text{ }\mu\text{K}$  [5]. The atoms are excited to a coherent superposition of Rydberg states in the presence of a very small electric field. After a small delay time intended to allow the superposition to evolve, a rapid pulse of the electric field is applied. At very large values of the electric field, the excited electrons are pushed off their atoms, across an intervening empty space, and into a detector, where the current produced is measured. This information is summarized in a timing diagram of the experiment, shown in Figure 1.1

The atoms must be cooled to such low temperatures in order to avoid the occurrence of significant decoherence during the delay time that would result from interatomic collisions. The low kinetic energy of atoms at this temperature allows for approximating them as stationary, as their motion over the course of the ex-

periment is small relative to their interatomic distances. By minimizing the kinetic energy, we minimize the probability of interatomic collisions occurring, and thus, the decoherence in the initial superposition. To achieve these temperatures, laser cooling techniques are used to cool Rydberg atoms in a Magneto Optical trap, with  $10^6$  atoms confined to region of diameter .5 mm [11].

We choose to excite the atoms to a superposition of the  $46D_{5/2}$ ,  $|m_j| = \frac{1}{2}$  and the  $46D_{5/2}$ ,  $|m_j| = \frac{3}{2}$  states in the presence of a small, initial electric field.<sup>1</sup> The excitation scheme used is depicted in Figure 1.2. The cooling lasers constantly cycle the atoms between the 5S and 5P states. The lasers tuned to this transition possess a wavelength of  $\lambda = 780$  nm. This also functions as the first step in the excitation scheme. Following this, the 5P atoms are excited to the 5D state using a 776 nm laser. Atoms in the 5D state will eventually fluoresce to the 6P state, with a lifetime on the order of 200 ns. From the 6P state, the atoms are finally excited to the selected 46D state using a 1022 nm laser. Due to energy time uncertainty, by confining this pulse in time, we are able to increase its bandwidth. So, we confine the pulse in time so that the uncertainty in energy covers both the  $46D_{5/2}$ ,  $|m_j| = \frac{1}{2}$  and the  $46D_{5/2}$ ,  $|m_j| = \frac{3}{2}$  states, thus achieving a coherent superposition [12].

By measuring the current produced by the atoms, we are approximately measuring the energy states of the atom at ionization, as higher energy atoms tend to ionize before lower energy atoms. Thus, electrons from higher energy atoms are expected to be detected earlier in time than those from lower energy atoms. Preliminary experimental investigations into similar problems have shown evidence that the energy distribution possess a large dependence on the delay time. We aim to investigate this further by treating the delay time as our independent variable. The

---

<sup>1</sup>For a discussion of the physical interpretation of these labels, see Section 3.1

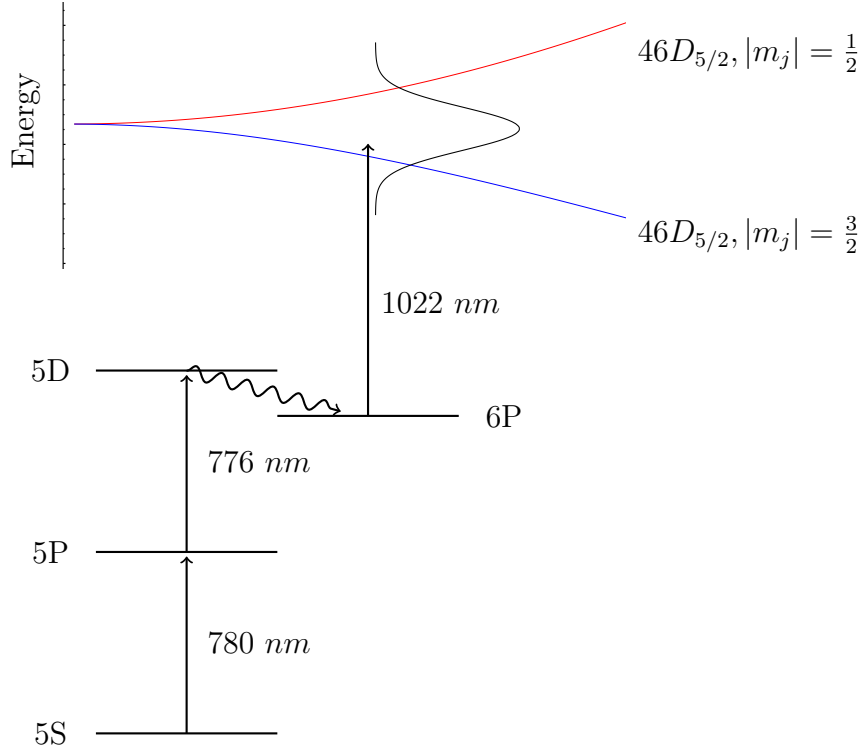


**Figure 1.2:** The excitation scheme used to excite to a superposition of Rydberg states.

energy distribution is also known to be sensitive to the rate at which the electric field is increased, known as the slew rate. For this experiment, a constant slew rate of 1 V/cm·ns is used.

The primary work of this thesis is to develop the necessary tools to simulate this experiment. We then compare the results of this simulation to those attained in the experiment, which is performed by our colleagues at Bryn Mawr College.

# Chapter 2

## Theoretical Introduction to the Stark Effect

### 2.1 A Model

To begin calculating the energy distribution of the atoms at ionization, we must first understand how the energy states of the atom themselves behave when subjected to an electric field. In order to probe the qualitative behaviour of the energy states of the atom, we first develop a simple model of two interacting energy levels [13]. Consider a system consisting of 2 energy states:  $|1\rangle$  and  $|2\rangle$ . The non-interacting Hamiltonian,  $\hat{H}_0$ , will be defined by the eigenvalue equations,

$$\hat{H}_0|1\rangle = E_1|1\rangle \tag{2.1}$$

$$\hat{H}_0|2\rangle = E_2|2\rangle. \tag{2.2}$$

Using the ordered basis  $\{|1\rangle, |2\rangle\}$ , this can be written in matrix form as

$$H_0 = \begin{pmatrix} \langle 1|\hat{H}_0|1\rangle & \langle 1|\hat{H}_0|2\rangle \\ \langle 2|\hat{H}_0|1\rangle & \langle 2|\hat{H}_0|2\rangle \end{pmatrix} = \begin{pmatrix} E_1 & 0 \\ 0 & E_2 \end{pmatrix}. \tag{2.3}$$

In order to account for the presence of an electric field, we must introduce a

perturbation term to the Hamiltonian. In atomic units, such a Hamiltonian takes the form

$$\hat{H} = \hat{H}_0 + \hat{V} \quad (2.4)$$

where  $\hat{V}$  is the perturbation matrix [14]. We will suppose that the diagonal terms of this matrix are constant with the electric field, and the off diagonal terms are linear in the electric field.<sup>1</sup> The perturbed Hamiltonian can thus be written as

$$H = \begin{pmatrix} \omega_1 & \delta e^{-i\phi} \\ \delta e^{i\phi} & \omega_2 \end{pmatrix}, \quad (2.5)$$

where  $\delta$  has an implied linear dependence on the electric field,  $F$ , and we have made the definitions

$$\omega_1 = E_1 + \langle 1|V|1\rangle \quad (2.6)$$

$$\omega_2 = E_2 + \langle 2|V|2\rangle \quad (2.7)$$

$$\langle 1|V|2\rangle = \delta e^{-i\phi}, \quad (2.8)$$

which are consistent with the assumptions made about the form of  $V$ . This Hamiltonian will serve as our model of two interacting energy states.

---

<sup>1</sup>Understanding why these conditions are imposed on the perturbation matrix requires looking ahead to (3.4), the actual perturbation matrix for Rydberg atoms in an electric field.

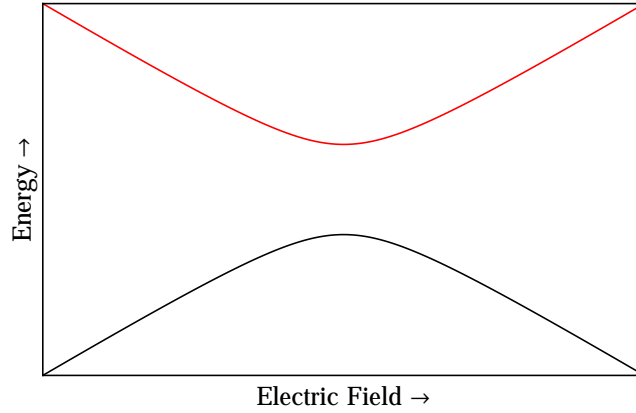


**Figure 2.1:** A plot of the eigenenergies of our idealized model of interacting energy states. In red is the plot of our first eigenvalue,  $E'_1$ . In black is the plot of our second eigenvalue,  $E'_2$ . See (2.9) and (2.10).

## 2.2 Interpreting the Model

We can easily solve for the eigenvalues of the matrix in (2.5) to find the observable energies of this system. They are:

$$E'_1 = \frac{1}{2} \left( \omega_1 + \omega_2 + \sqrt{(\omega_1 - \omega_2)^2 + 4\delta^2} \right) \quad (2.9)$$

$$E'_2 = \frac{1}{2} \left( \omega_1 + \omega_2 - \sqrt{(\omega_1 - \omega_2)^2 + 4\delta^2} \right). \quad (2.10)$$

In Figure 2.1, we show these eigenvalues as a function of the electric field. This model captures two essential features that are observed in Rydberg atom systems.

First, we see that the energy levels possess a nontrivial dependence on the electric field. Consequently, in our experiment, as the electric field surrounding the Rydberg atom changes, so too will the values of its observable energies. This is known as the Stark effect. The second feature seen in Figure 2.1 is that, while the energy levels are initially on a trajectory that appears to have them cross, they “bend” away from each other. This is known as an avoided crossing. The significance of avoided crossings is explained in Chapter 5.



# Chapter 3

## Numerically Computing Stark Maps

### 3.1 The Hamiltonian of a Rydberg Atom

We now compute the Hamiltonian, and thus, the eigenenergies and energy eigenstates, of a Rydberg atom subject to an electric field. We first review the conventions used when describing the energy levels of an atom. For our purposes, there are four quantum numbers required to fully specify an energy level of an atom in the presence of an electric field. The first of these is the principle quantum number,  $n$ , which is a measure of the radial distance from the nucleus of the atom. The second of these,  $\ell$ , is the orbital angular momentum of an electron inhabiting that energy state. In most cases, we will use the standard  $S, P, D, F, \dots$  notation to denote orbital angular momenta of 0, 1, 2, 3, .... The third quantum number,  $j$ , is the total angular momentum of an electron in the energy state. The total angular momentum is given by  $j = \ell + s$ , where  $s$  is the spin of the electron. The  $j$  value will be denoted by a subscript on the letter giving the orbital angular momentum. Finally, the last quantum number,  $m_j$ , measures the projection of the total angular momentum along the axis aligned with the electric field. We will often use  $|m_j|$  rather than  $m_j$  because, as we will see shortly, the sign of  $m_j$  does not effect the



measurable energies of the state for our purposes.

It is clear that any energy level may be specified by the ket  $|n, l, j, m_j\rangle$ . Because the set of all such kets is orthonormal, we use this set as the basis for the Hamiltonian of our atom. In order to find the Hamiltonian for a Rydberg atom, we must evaluate (2.4). The unperturbed Hamiltonian is, unsurprisingly, defined by the eigenvalue equation

$$\hat{H}_0|n, l, j, m_j\rangle = E_{n,l}|n, l, j, m_j\rangle. \quad (3.1)$$

Care must be taken in evaluating  $E_{n,l}$ . As explained in Chapter 1, the properties of Rydberg atoms are often similar to those of Hydrogen, but at a larger scale. Thus, an initial guess for the observable energies may be  $E_n \approx -\frac{13.6}{n^2}$  eV. However, we also expect small deviations from the hydrogenic case, as there is a small amplitude for the valence electron to reside within the positively charged core of the Rydberg atom, where deviations from the Coulomb potential of the Hydrogen atom are no longer negligible. These deviations can be accurately accounted for using quantum defect theory [1]. Quantum defect theory predicts that the energy of an unperturbed state is described by the equation

$$E_{n,l} = -\frac{13.6}{(n - \delta_l)^2} \text{eV}. \quad (3.2)$$

The  $\delta_l$  appearing in this equation are experimentally determined parameters that depend only on the orbital angular momentum of the electron that are known as the quantum defects. It follows from this equation that the matrix elements for the

unperturbed Hamiltonian are given by

$$\langle n, l, j, m_j | H_0 | n', l', j', m'_j \rangle = -\delta_{n,n'} \delta_{l,l'} \delta_{j,j'} \delta_{m_j,m'_j} \frac{1}{2(n - \delta_l)^2} \quad (3.3)$$

where we have now begun using atomic units.

The perturbation matrix,  $V$ , is given by the potential of the interaction with the electric field. For an electric field of magnitude  $F$  in the  $\hat{z}$  direction, the potential energy of this interaction is given by  $V = Fz = Fr \cos \theta$ , where we have simply casted to spherical coordinates to achieve the last equality. By adding in total  $\delta_{m_j,m'_j}$  and  $\delta_{l,l'\pm 1}$  to enforce selection rules, and coefficients to cast the angular terms to the same basis, we see that the matrix elements may be found using [15]

$$\begin{aligned} \langle n, l, j, m_j | V | n', l', j', m'_j \rangle &= \delta_{m_j,m'_j} \delta_{l,l'\pm 1} \langle n, l | r | n', l' \rangle F \times \\ &\sum_{m_l=m_j \pm \frac{1}{2}} \langle l, \frac{1}{2}, m_l, m_j - m_l | j, m_j \rangle \langle l', \frac{1}{2}, m_l, m_j - m_l | j, m_j \rangle \langle l, m_l | \cos \theta | l', m_l \rangle. \end{aligned} \quad (3.4)$$

According to (2.4), we simply add (3.3) and (3.4) to find the Hamiltonian for our system. Notice that this equation only depends on the  $|m_j|$  rather than  $m_j$ , so the energy levels for the  $\pm m_j$  states are degenerate at all values of the electric field.

## 3.2 Solving for the Matrix Elements

Solving (3.3) and (3.4) to find the matrix elements of the Hamiltonian for the perturbed system is quite challenging. First, we see that there is an overall  $\delta_{m_j,m'_j}$ , so we may generate the Hamiltonians for each value of  $m_j$  separately. We solve (3.3) by using quantum defects attained from various sources [16–18].

To solve (3.4), we first consider the expression within the sum. The first 2 coef-

ficients in the sum,  $\langle l, \frac{1}{2}, m_l, m_j - m_l | j, m_j \rangle$  and  $\langle l', \frac{1}{2}, m_l, m_j - m_l | j, m_j \rangle$ , are known as Clebsch-Gordon Coefficients [19]. The last term in the sum,  $\langle l, m_l | \cos \theta | l', m_l \rangle$ , is the angular part of the matrix element. The analytic solution is [15]

$$\langle l, m_l | \cos \theta | l - 1, m_l \rangle = \left( \frac{l^2 - m_l^2}{(2l + 1)(2l - 1)} \right)^{1/2} \quad (3.5)$$

$$\langle l, m_l | \cos \theta | l + 1, m_l \rangle = \left( \frac{(l + 1)^2 - m_l^2}{(2l + 3)(2l + 1)} \right)^{1/2}. \quad (3.6)$$

The radial term,  $\langle n, l | r | n', l' \rangle$ , is the only non-trivial part remaining. Writing this as an integral yields

$$\langle n, l | r | n', l' \rangle = \int_0^\infty R_{n,l}^* r R_{n',l'} r^2 dr, \quad (3.7)$$

where  $R$  is a solution to the radial part of the Schrödinger equation,

$$\frac{d^2 R}{dr^2} + \frac{2}{r} \frac{dR}{dr} + 2(E - V) R - \frac{l(l + 1)}{r^2} R = 0, \quad (3.8)$$

and the factor of  $r^2$  comes from the differential volume element [20]. We express this equation with the variables  $x = \ln r$  and  $X = \sqrt{r} R$  to get

$$\frac{d^2 X}{dx^2} = g(x) X. \quad (3.9)$$

where  $g(x) = (l + \frac{1}{2})^2 + 2(V - E)e^{2x}$  [15]. A second order differential equation in this form can be solved using the Numerov method [21]. Numerov's method states that, given two initial values for  $X$

$$X_{i+1} = \frac{X_{i-1} \left( g_{i-1} - \frac{12}{h^2} \right) + X_i \left( 10g_i + \frac{24}{h^2} \right)}{\frac{12}{h^2} - g_{i+1}}, \quad (3.10)$$

where  $g_i = g(x_i)$ , and  $h$  is the step size. The boundary conditions imposed are  $x_0 = 10^{-10}$  and  $x_1 = 10^{-5}$ , though the integration was quite insensitive to this. By requiring that the squared modulus of the wave function integrated over all space achieves unity, we find that the normalization constant,  $N$ , is given by

$$N = \left( \int_0^\infty X^* X r^2 dr \right)^{-1/2}. \quad (3.11)$$

Writing (3.7) in terms of  $X$ , and casting the problem to the discrete regime, we solve for the radial part of the matrix element with

$$\langle n, l | r | n', l' \rangle = \frac{\sum_i X_i^* X'_i r_i^2}{\left( \sum_i X_i^2 r_i^2 \sum_j X_j'^2 r_j^2 \right)^{-1/2}}, \quad (3.12)$$

where we have used  $X = r^{1/2} R_{n,l}$  and  $X' = r^{1/2} R_{n',l'}$ . The information detailed in this section allows us to solve (3.4), and, in conjunction with (3.3), find all matrix elements of the perturbed Hamiltonian.

### 3.3 A Sample Stark Map

By diagonalizing the Hamiltonian solved for in Section 3.2, we may read the eigenvalues off the diagonal elements to find the observable energies of a Rydberg atom in the presence of an electric field. At a single field, this would result in the energy level diagram of the atom. By solving for the eigenvalues at many fields, we are able to observe the dependence of the energies on the electric field. Such a plot, showing the energy level diagrams as a function of the electric field, is called a Stark map. An example of a Stark map is shown in Figure 3.1.

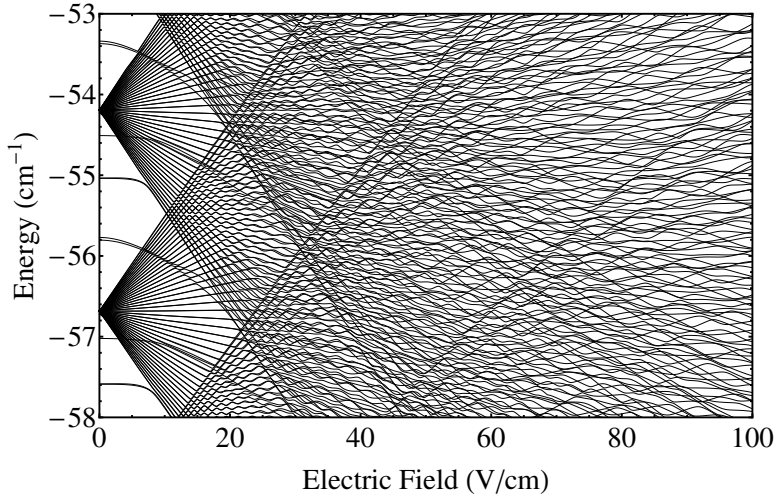


**Figure 3.1:** The Stark map for  $^{85}\text{Rb}$  around the  $n = 43$  and  $n = 44$  manifolds for the  $|m_j| = \frac{1}{2}$  states. Shows the dependence of the observable energies on the applied electric field.

There is much to be said about Figure 3.1. First, as mentioned in Section 3.2, we do not need to consider all  $m_j$  states at the same time. Consequently, we have only generated the Hamiltonians for the  $|m_j| = \frac{1}{2}$  states here, though other values of  $|m_j|$  would generate nearly identical Stark maps. The exception to this is that a few states may not be present in the map for larger  $|m_j|$ , due to the constraint that  $|m_j| \leq j$  for physical states.

Perhaps the most striking feature of Figure 3.1 is that, at relatively small values of the electric field, many of the states appear to “fan” out as the field is increased. There are 2 such “fans” visible in this figure, beginning at roughly  $E = -54.2 \text{ cm}^{-1}$  and  $E = -56.7 \text{ cm}^{-1}$ . These are known as manifolds. Typically, a manifold is composed of large  $l$  states, approximately the  $f$  states and above, of the same  $n$  value. Shown here are the  $n = 43$  (bottom) and  $n = 44$  (top) manifolds. The states that do not lie within a manifold are the lower angular momentum ( $s, p, d$ ) states of larger  $n$  values. These are detached from their manifold due to the large quantum

defects observed for low  $\ell$  states, which result from the larger amplitude for these states to lie within the ionic core of the atom.

While at this scale it may be difficult to discern, when two adjacent states appear to cross in this Stark map, they are actually deflecting away from each other. These are the avoided crossings predicted by the model presented in Chapter 2.



# Chapter 4

## Introduction to Landau-Zener Theory

### 4.1 Model of Population Dynamics at Avoided Crossings

Thus far, we have studied the behaviour of the energy levels in response to electric fields. We now ask the slightly different question, what happens to the *amplitude* in these energy levels as the electric field is varied over time? This is of significant importance when considering the ionization experiment describe in Section 1.2, as answering this allows us to track the distribution of the amplitude across the energy levels as the ionization pulse is applied.

To begin answering this question, we again return to the model of two energy states subject to a perturbation, given by (2.5) [13]. For convenience, this equation is repeated here.

$$H = \begin{pmatrix} \omega_1 & \delta e^{-i\phi} \\ \delta e^{i\phi} & \omega_2 \end{pmatrix} \quad (4.1)$$

To see how this model Hamiltonian was developed, and the definitions being used,



refer to Section 2.1. In this Section, we slightly change our interpretation of the terms in this Hamiltonian. More specifically, we follow the reference and take the  $\langle 1|V|1\rangle$  and  $\langle 2|V|2\rangle$  terms in  $\omega_1$  and  $\omega_2$  to have a linear dependence on the electric field, rather than  $\delta$  [13].

The energy eigenstates available to the system are given by the eigenvectors of this matrix. If we let  $|E'_1\rangle$  correspond to the eigenvalue  $E'_1$  and  $|E'_2\rangle$  correspond to the eigenvalue  $E'_2$ , then the eigenstates are given by

$$|E'_1\rangle = \cos\left(\frac{\theta}{2}\right) e^{-\frac{i\phi}{2}}|1\rangle + \sin\left(\frac{\theta}{2}\right) e^{\frac{i\phi}{2}}|2\rangle \quad (4.2)$$

$$|E'_2\rangle = -\sin\left(\frac{\theta}{2}\right) e^{-\frac{i\phi}{2}}|1\rangle + \cos\left(\frac{\theta}{2}\right) e^{\frac{i\phi}{2}}|2\rangle, \quad (4.3)$$

where we have defined  $\tan\theta = \frac{2\delta}{\omega_1 - \omega_2}$ .

To quantitatively described the evolution of the amplitude in these states over time, we must solve the time dependent Schrödinger equation

$$H|\Psi(t)\rangle = i\frac{\partial|\Psi(t)\rangle}{\partial t}. \quad (4.4)$$

Following Landau [22] and Zener [23], we propose the solution

$$|\Psi(t)\rangle = C_1(t)e^{-i\int_0^t \omega_1 dt'}|1\rangle + C_2(t)e^{-i\int_0^t \omega_2 dt'}|2\rangle. \quad (4.5)$$

By substituting this into (4.4) and decoupling the resulting differential equations, we see that  $|\Psi(t)\rangle$  is a solution if the constants  $C_1$  and  $C_2$  obey the differential

equations

$$\ddot{C}_1 - i(\omega_1 - \omega_2)\dot{C}_1 + \delta^2 C_1 = 0 \quad (4.6)$$

$$\ddot{C}_2 + i(\omega_1 - \omega_2)\dot{C}_2 + \delta^2 C_2 = 0 \quad (4.7)$$

We may now solve for the probability of a system with a known initial state, which we will choose to be  $|E'_2\rangle$ , to be found in  $|E'_1\rangle$  at some later time. The probability of this state being found in  $|E'_1\rangle$  at a time  $t_f$  is given by

$$Pr(|E'_1\rangle) = |\langle\Psi(t_f)|E'_1(t_f)\rangle|^2 \quad (4.8)$$

where  $|\Psi(t)\rangle$  satisfies the condition  $|\Psi(t_i)\rangle = |E'_2\rangle$ . If  $\omega_1$  and  $\omega_2$  evolve linearly with time,  $t_i = -\infty$ , and  $t_f = \infty$ , we may solve (4.6) and (4.7), and thus (4.8). This yields the solution

$$Pr(|E'_1\rangle) = \exp\left(-\frac{2\pi}{\frac{dq}{dt}} \frac{\delta^2}{\left.\frac{d|\omega_1 - \omega_2|}{dq}\right|_{q_c}}\right), \quad (4.9)$$

where  $q_c$  is the value of the parameter at which the crossing occurs [22, 23]. This is known as the Landau-Zener formula.

## 4.2 Solving the Landau-Zener Formula

In the idealized case explained in Section 4.1, we have seen that (4.9) may be used to calculate the probability of a transition occurring when a state traverses an avoided crossing. First, we note that the probability of a transition is not zero. In the context of ionizing a Rydberg atom, this means that if an atom is prepared in a

selected energy state, it may not ionize in that same state. To gain a greater intuitive understanding of the implications of (4.9), we study the terms in the equation more closely.

We were purposely vague about where exactly  $q_c$  occurs. The natural definition is that it occurs at the minimum in the separation of the perturbed energy levels. To find this minimum, we set the derivative of the difference of the eigenvalues given in (2.9) and (2.10) to 0. That is,

$$\frac{d \left( \sqrt{(\omega_1 - \omega_2)^2 + 4\delta^2} \right)}{dq} = 0. \quad (4.10)$$

Solving this, we find that at the crossing,

$$\omega_1(q_c) - \omega_2(q_c) = 0. \quad (4.11)$$

We may then plug this result back into the expression for  $E'_1 - E'_2$  to see that, at the crossing,

$$E'_1 - E'_2 = 2\delta \quad (4.12)$$

This allows for any easy way to calculate the  $\delta$  appearing in (4.9); we simply subtract the perturbed energy values given by a Stark map, and divide the result by 2.

We next analyse the  $\omega_1$  and  $\omega_2$  term appearing in the Landau-Zener Formula. We know that  $\omega_1$  and  $\omega_2$  are linear in  $q$  from their definitions. We must find two points that lie on the line in order to fully describe it. We can evaluate the definition of  $\omega_1$ , (2.6), at  $q = 0$  to see that  $\omega_1(0) = E_1$ . A second point on this line may be

found using (2.9) and (4.11). This gives

$$E'_1(q_c) = \frac{1}{2}(\omega_1(q_c) + \omega_2(q_c) + 2\delta) \quad (4.13)$$

$$= \omega_1 + \delta \quad (4.14)$$

$$\Rightarrow \omega_1(q_c) = E'_1 - \delta, \quad (4.15)$$

which is the point halfway between the perturbed energy states at the crossing.

Using similar deductions to find points on  $\omega_2$ , we may plot the lines for  $\omega_1$  and  $\omega_2$ , as shown in Figure 4.1. We see that we can easily gather difference in the slope of these lines from a Stark map, providing us with the  $\frac{d|\omega_1 - \omega_2|}{dq}$  term. The final term involved in the Landau-Zener equation is  $\frac{dq}{dt}$ , which is a parameter set by the experimenter known as the slew rate, which is the rate at which the electric field is being increased. Thus, all terms necessary to evaluate the Landau-Zener formula are easily attainable from a Stark map, or, in the case of the slew rate, experimentally determined.

The interpretation of the terms in this equation also allows us to discuss its qualitative interpretation. From the  $\delta$  term appearing in the numerator of the exponential, we see that crossings with a very small energy difference between the two states have an increased probability of a diabatic transition occurring relative to crossings with a smaller energy difference. Moreover, from the  $\frac{d|\omega_1 - \omega_2|}{dq}$  term, we see that if the states are approaching each other very rapidly, then the probability of a diabatic transfer also increases relative to states undergoing a more drawn out crossing. Finally, the  $\frac{dq}{dt}$  term shows that, if the experimenter ramps the field faster, then there is a greater probability of a diabatic transfer occurring. The probability of a diabatic transfer occurring is incredibly sensitive to all of these terms, as they

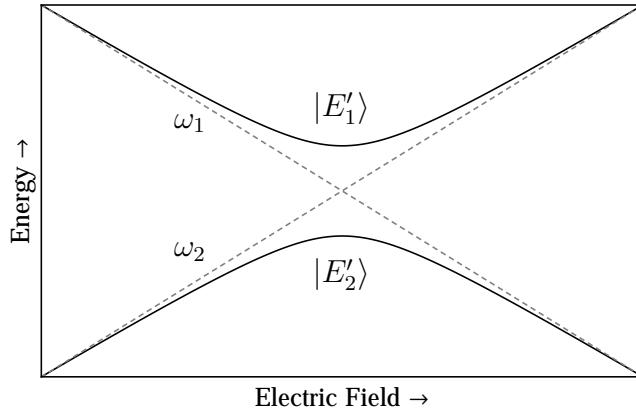


**Figure 4.1:** In black, solid lines, we have again plotted the eigenenergies of our idealized model of interacting energy states. In grey, dashed lines, we have plotted  $\omega_1$  and  $\omega_2$ .

appear in the exponential of 4.9.

### 4.3 Evolving a State through Ionization

We now present an algorithm for evolving a state through ionization, using the results of Section 4.1 and Section 4.2 [24]. Suppose we are given an the initial state of a Rydberg atom. We then subject the atom to an increasing electric field until the electric field strong enough to ionize the atom. Pictorially, we view this as beginning with a state on the left side of our Stark map (see Figure 3.1). As the electric field is increased, we sweep across the map from left to right, until we reach the electric field at which the atom ionizes<sup>1</sup>.

We see that, as we perform this sweep, a state will traverse many avoided crossings, and thus, the amplitudes will spread over many states. The amplitude residing in each state could be calculated using the Landau-Zener formula as follows. First, we step through the field from left to right. Then, if an avoided crossing is en-

---

<sup>1</sup>For a more detailed discussion of where this ionization takes place, see Section 5.2

countered, we calculate the probability of a transfer occurring at the crossing, using the Landau-Zener formula and the methods from Section 4.2. We then use that probability to reallocate the amplitude in our state vector into the correct states. Following this, we evolve the phases of each component of the state vector, using the energy of the state at the current value of the electric field. Finally, we repeat this process until the state is ionized. An implementation of such an algorithm has been performed in Ref. [24].

Many difficulties are encountered when applying this approach to our problem. The first problem is that the Landau-Zener formula provides no phase information. That is, it does not give the amplitude of a transfer occurring, rather, it gives the squared modulus of it. An attempted remedy to this solution is numerically integrating (4.6) and (4.7), rather than using the Landau-Zener formula. However, the phase was found to be incredibly sensitive to our arbitrary choice of where to start and end the integration. The second problem encountered was that the Landau-Zener formula was derived for an idealized case that is not often realized in our Stark map. This causes us to be sceptical of results attained in the less than ideal cases that are found throughout the Stark map. Finally, there are instances in the Stark map where we see three or more energy levels undergoing avoided crossings at the same time. The Landau-Zener formula offers no qualitative or quantitative insight into such cases. While there have been quantitative descriptions of multilevel crossings, the calculations are significantly more complicated [25–27]. For these reasons, a different approach is needed to evolve our state through ionization.



# Chapter 5

## Alternative to Landau Zener Theory

### 5.1 The Algorithm

We now present a new algorithm for evolving the state through ionization, following the approach taken in Ref. [28]. The Hamiltonian of an atom subject to a changing electric field is quite clearly time dependent.<sup>1</sup> However, over a small time scale, the Hamiltonian may be approximated as constant in time. From non-relativistic quantum mechanics, we know that for a time independent Hamiltonian, states are evolved through time by applying the time evolution operator, or

$$|\psi(t)\rangle = e^{-i\hat{H}t/\hbar}|\psi(0)\rangle. \quad (5.1)$$

So, to evolve the initial state in time, we approximate the Hamiltonian as constant over a short time step  $\Delta t$  using (5.1). That is, we use the approximation

$$|\psi(t_0 + \Delta t)\rangle = e^{-i\hat{H}(t_0)\Delta t/\hbar}|\psi(t_0)\rangle. \quad (5.2)$$

---

<sup>1</sup>See (3.4)



Beginning with a given initial state vector, we iteratively apply this formula until we reach a time where the atom is considered to be ionized.

This algorithm has many advantages over the algorithm explained in Section 4.3. First, the phase information need not be dealt with explicitly, as (5.2) deals directly with amplitudes rather than probabilities, unlike the Landau-Zener formula. Additionally, though we know avoided crossings are the areas where most population transfer occurs, they too do not need to be dealt with explicitly. So, we do not need to worry about cases where the crossings are less than ideal, or cases where three or more states are interacting at the same time. Finally, all parts of this problem are “embarrassingly” parallel, which leads to a tractable computation time. This will be explained more in the following section.

While the details of performing the computation are explained in the next section, we first would like to justify its use. To test this algorithm, we have selected a particularly well behaved avoided crossing from our Stark map and have calculated the probability of a diabatic transfer occurring using this algorithm. In Figure 5.1, we compare these values to the probability of transfer given by the Landau-Zener formula, using many different values of the slew rate. We see very good agreement between the two methods, especially at large slew rates. Because the time step of the numerical calculation is set to the resolution of the Stark map divided by the slew rate, at lower slew rates, the time step increases. This is likely the source of disagreement between that is observed for small slew rates.

## 5.2 Performing the Computation

There are two steps to solving (5.2): Generating the time evolution operator, and applying it to our state. We first generate all the time evolution operators. In

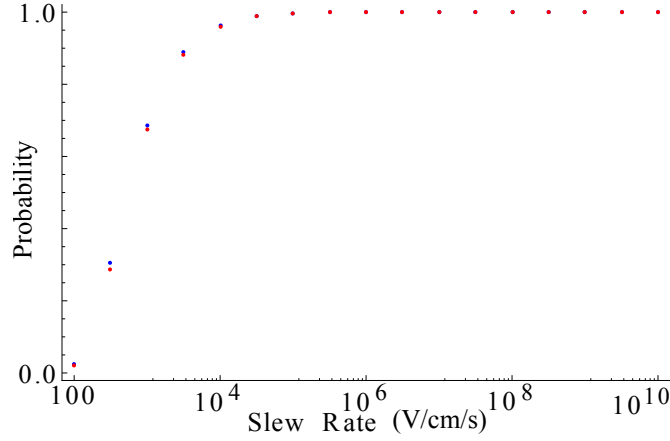


**Figure 5.1:** The probability of a diabatic transfer occurring as the system is evolved through an avoided crossing for many different slew rates. The blue dots show the probability of transfer given by the Landau-Zener formula. The red dots show the probability of transfer given by the algorithm described in Section 5.1.

order to evolve our state in time, we must ensure that the time evolution operators are given in the same basis as  $|\psi\rangle$ . To do this, we choose to time evolve in the basis of eigenstates of the Hamiltonian when no electric field is applied, or the zero field basis. This is achieved by performing the matrix exponentiation in the current field basis, and then transforming the result to the zero field basis, using the formula

$$U_0(t_0) = S_0 e^{-iH_c(t_0)\Delta t/\hbar} S_0^T. \quad (5.3)$$

In this equation, the subscript 0 denotes matrices in the zero field basis, the subscript  $c$  denotes matrices in the current field basis, and  $S$  is the matrix of eigenvectors of  $H(t_0)$ . As the matrices may be quite large, both generating  $H$  and performing (5.3) can potentially require a large amount of time to compute. However, the time evolution operators may be generated in parallel quite easily, as they are independent of each other. This significantly reduces the computation time required.

Following the generation of the time evolution operators, we evolve the state

through time using (5.2), with our newly evaluated time evolution operators. For the sake of optimizing computing time, this is done as the time evolution operators are being generated. Alternatively, this could also be done in parallel by multiplying sequential time evolution operators together before multiplying by the state vector. That is, we can view the iterative use of (5.2) as evaluating the following equation:

$$|\psi(t_f)\rangle = U(t_f - \Delta t)U(t_f - 2\Delta t)\dots U(t_0 + \Delta t)U(t_0)|\psi(0)\rangle \text{ (n times)}, \quad (5.4)$$

where n is the number of time steps involved in the calculation. By sectioning the multiplication of time evolution operators on the right hand side and multiplying them together in order, we could potentially perform the evolution of the state in parallel.

We have not yet made rigorous the notion of where ionization occurs, and thus, when to terminate our program. One approximation is given by the classical ionization limit, given by

$$E_{ionization} = -6.12\sqrt{F} \quad (5.5)$$

where energy is measured in  $\text{cm}^{-1}$  from threshold, and the electric field is measured in  $\text{V}/\text{cm}$ . Currently, we model ionization as occurring at a single electric field for all energy states near the area where most of the population encounters the classical ionization limit. In the near future, we plan to implement a more realistic model of this ionization.<sup>2</sup>

---

<sup>2</sup>See Chapter 7.

### 5.3 The Detector

In the next chapter, we will present the result of our calculation, and compare them to the experimental results when possible. In order to perform this comparison, though, we must be able to model the detector used in experiment. While admittedly crude, the model used is explained briefly below.

First, we assign a Gaussian distribution to all elements in both the  $|m_j| = \frac{1}{2}$  and the  $|m_j| = \frac{3}{2}$  state vectors at ionization. These Gaussian peaks are assigned such that the area beneath each peak is given by the squared modulus of the amplitude in the corresponding state. Additionally, the mean of each peak is set to occur at the field value where the amplitude in that state had ionized, according to the classical ionization limit. The standard deviation,  $\sigma$ , of the distribution allows us to parameterize the uncertainties in the field at which the atom is ionized and the arrival time at the detector.

After defining the Gaussian peaks, we numerically integrate over all space, summing the amplitudes from all peaks from both the  $|m_j| = \frac{1}{2}$  and the  $|m_j| = \frac{3}{2}$  state vectors. To perform this numerical integration, we must choose a finite  $\Delta x$  as the integration variable. This parameter may be viewed as a measure of how near in ionization field, or equivalently, arrival time at the detector, two amplitudes must be in order to display interference effects. The parameters  $\Delta x$  and  $\sigma$  are chosen to provide a best fit to the experimental data.



# Chapter 6

## Results

### 6.1 Path to Ionization

In this chapter, we present the results of our simulation juxtaposed with experimental results attained at Bryn Mawr College. In our simulation, we have considered all states with  $n$  values between 42 and 47, with all physical  $n = 48, 49, 50$   $S, P$ , and  $D$  states included as well. States excluded from the calculation did not significantly interact with any state that possessed a substantial amount of amplitude before ionization occurred, and were thus excluded to decrease the computation time. To initialize the wave function, we set the  $n = 46D_{5/2}$  state to unity in both the  $|m_j| = \frac{1}{2}$  and  $|m_j| = \frac{3}{2}$  states. It was found that any initial phase accrued during the delay time carried through the ionization process, so, the state was evolved through the ionization ramp before applying this phase difference. We have used a constant slew rate of  $10^9$  V/cm·s, which is approximately equal to that used by the experimenters at Bryn Mawr.

The dynamics of the population during the ionization ramp are shown in Figure 6.1. On the left of the figure, we see that most of the population remains in its initial state until it collides with the manifold, at approximately 15 V/cm. At this point, the population splits into two main groups of energy levels, and these groups

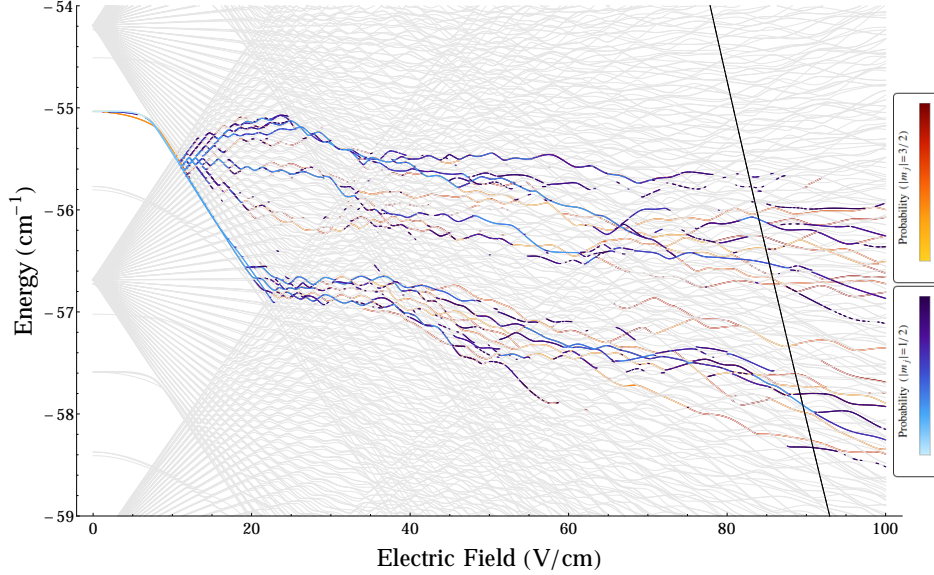


**Figure 6.1:** The amplitude tracked through the ionization ramp on a Stark map. The states in blue colors contain  $|m_j| = \frac{1}{2}$  population, and those in red colors contain  $|m_j| = \frac{3}{2}$  population. The black line towards the right of the figure gives the classical ionization limit, which approximates the location where ionization occurs.

remain approximately isolated until the classical ionization limit is reached.

## 6.2 Ionization Currents

We now attempt to reproduce the current measured in experiment with our simulation. To produce an ionization current from our simulation results, we use the model of the detector given in Section 5.3. The results are shown in Figure 6.2.

We observe a two peak structure in both results, which are in qualitative agreement. In retrospect, we could have predicted this two peak pattern from viewing Figure 6.1. In the discussion of that figure, we noted that the population had split into two groups which remained isolated until ionization. In Figure 6.2, each peak corresponds to one of these groups. More specifically, the left peak in the ionization

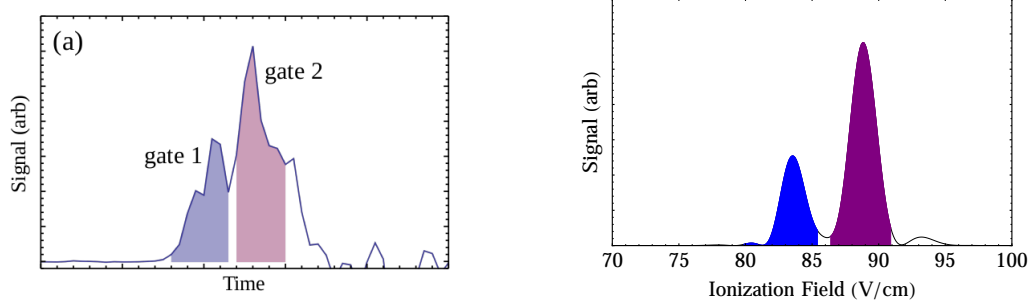


**Figure 6.2:** Left: Experimental Ionization Current. Right: Simulated Ionization Current. A two peak distribution is observed.

current, which arrived at the detector earlier in time, corresponds to the “upper” group of energy levels, as the states of higher energy ionize first. Likewise, the right peak in the ionization current corresponds to “lower” group of energy levels.

In generating Figure 6.2, we have plotted the ionization current for a single delay time. Next, we wish to observe how the ionization current changes as the initial phase difference is varied. To do this, we quantify the size of each peak by the area it encloses. The integration boundaries for each peak are shown by the colors in Figure 6.2. In Figure 6.3, we show how the size of the peaks depend on the initial delay time in both the experimental and simulated results.

Again, we observe a qualitative agreement between the simulated and experimental results, with the exception of a lack of decoherence effects observed in the simulation, which is to be expected. We also see that, as the delay time increases, the size of the peaks experience an oscillation that is  $\pi$  out of phase with each other, which is reminiscent of an interference experiment. This is discussed further in Section 6.4.



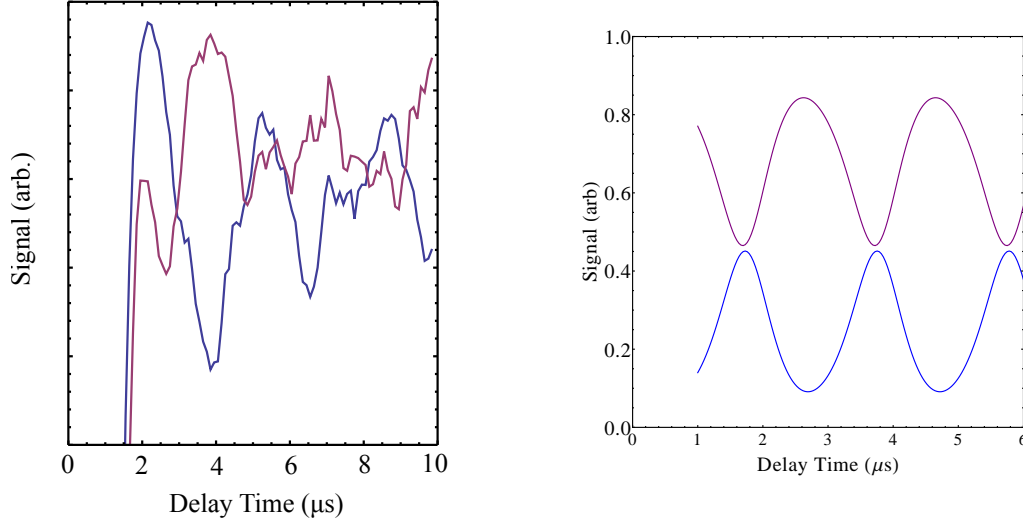


**Figure 6.3:** Left: Size of the peaks in the ionization current observed in experiment. Right: Size of the peaks in the simulated ionization current. We see  $\pi$  out of phase oscillations in both cases.

### 6.3 Comparison of Oscillation Frequencies

We know that the phase arises from the  $e^{i\Delta Et/\hbar}$  term from time evolving the initial state, where  $\Delta E$  is the separation between the states at the initial electric field. So, we expect the frequency of the oscillations in the peak size to increase as  $\Delta E$  increases. In Figure 6.4, we show a Stark map of the area between 0 V/cm and 1 V/cm that includes the two states in the initial superposition. We see that, as the electric field increases, so does the energy difference between the states. Thus, we expect the frequency of oscillations in the peak size to also increase as the initial field increases.

In Figure 6.5, we compare the oscillation frequencies of 1 of the peaks in the ionization current for many different initial fields for both the experimental and calculated results. It is clear in both the experimental and simulated data that, as the initial electric field increases, so does the frequency of the oscillations in the

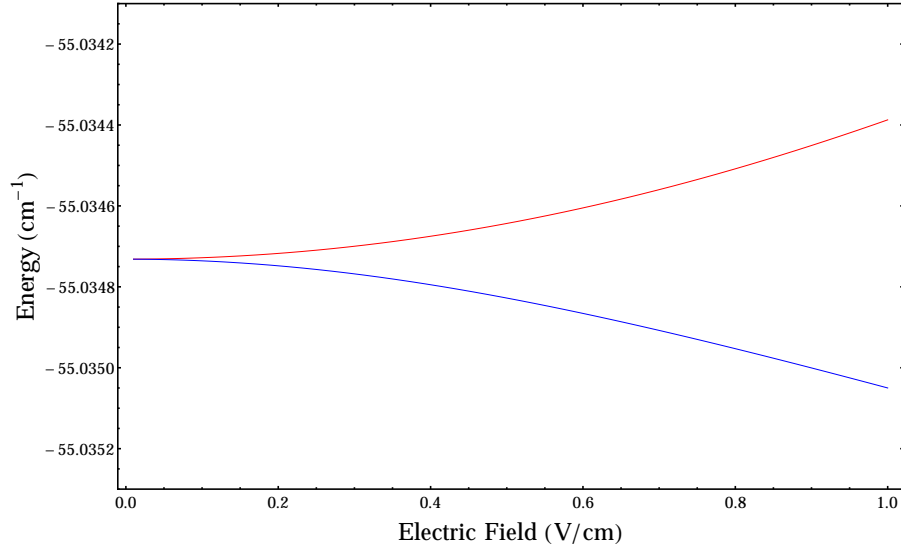


**Figure 6.4:** The low field Stark Map of the states in the initial superposition. The state in red is the  $46d, j = \frac{5}{2}, |m_j| = \frac{1}{2}$  state. The state in blue is the  $46d, j = \frac{5}{2}, |m_j| = \frac{3}{2}$  state.

ionization current, as expected. Though quantitative agreement is not observed, the ratios between the frequencies were found to be equal.

## 6.4 Discussion and Interpretation

As we have hinted earlier, we interpret this experiment as an interference experiment, similar to a Mach-Zehnder interferometer [29, 30]. In Figure 6.6, we show a diagram of a Mach-Zehnder interferometer.

There are three key steps in an experiment using a Mach-Zehnder interferometer that lead to an interference pattern. First, the amplitude is split into two groups. Second, a phase difference develops between the two groups of amplitude. Third, the groups of amplitude are brought back together. For example, in the case of a traditional Mach-Zehnder interferometer, the first beam splitter separates the amplitude into 2 groups, the different path length allows a phase difference to

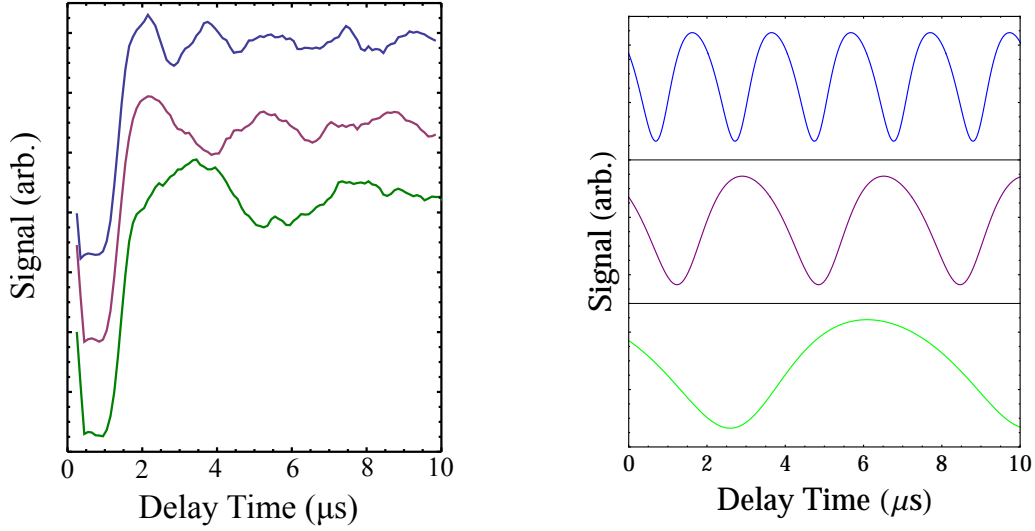


**Figure 6.5:** Comparison of the frequency of the oscillations observed for different values of the initial electric field. Oscillations for an initial field of  $F = .18975 \text{ V/cm}$  are shown in green,  $F = .276 \text{ V/cm}$  are shown in purple, and  $F = .3707 \text{ V/cm}$  are shown in blue.

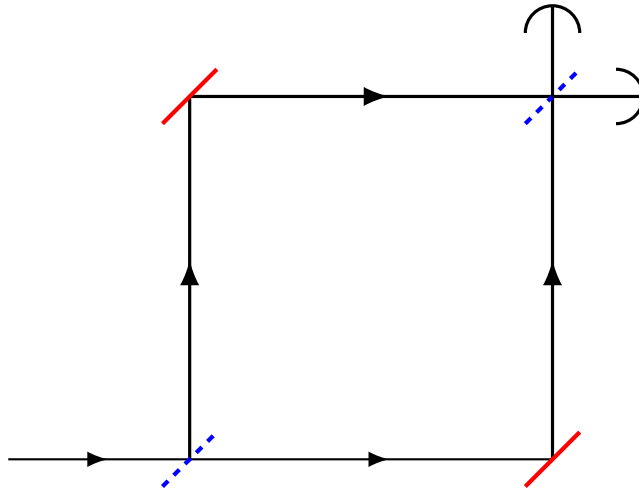


**Figure 6.6:** A Mach-Zehnder interferometer. The possible paths the amplitude can take is indicated by the black lines. The blue, dashed lines represent 50/50 beam splitters. The red, solid lines represent perfect mirrors.

develop, and finally, the last beam splitter recombines the two groups of amplitude.

To make the analogy to the Mach-Zehnder interferometer explicit, in our ionization experiment, the excitation of the initial superposition splits the population into two groups, the  $|m_j| = \frac{1}{2}$  and  $|m_j| = \frac{3}{2}$ , analogous to the first beam splitter. Then, due to the energy difference between the states, the delay time allows for a phase difference to develop between the two states, which is analogous to the different path length in each arm of the Mach-Zehnder interferometer. Finally, when the amplitude is ionized, it recombines with the amplitude ionized from the other  $|m_j|$  states, serving as the second beam splitter in a Mach-Zehnder interferometer. Thus, we see that this ionization experiment can be conceptually understood as a Mach-Zehnder interferometer.



# Chapter 7

## Future Work

### 7.1 Treatment of Ionization

The classical ionization limit is a quite poor approximation to where ionization occurs. While we have demonstrated qualitative agreement with the experimental results despite this, we would like to implement a more formal treatment of ionization. We plan to do this by calculating the ionization rate of each state in our Stark map, and using this rate to remove the appropriate amount of amplitude from our wave function when continuing to the next time step in the evolution. However, such a precise treatment is likely not needed. We believe that simply waiting to remove the amplitude from our state vector until the ionization rate reaches some threshold would serve as a good approximation of the process.

For a state expressed in the parabolic basis, the ionization rate,  $\Gamma$ , is given by the equation [28]

$$\Gamma = \frac{(4R)^{2n_2+m+1}}{n^3 n_2! (n_2 + m)!} \exp \left[ -\frac{2}{3}R - \frac{1}{4}n^3 F (34n_2^2 + 34n_2 m + 46n_2 + 7m^2 + 23m + \frac{53}{3}) \right]. \quad (7.1)$$

In this equation  $n_1, n_2, n$ , and  $m$  are the parabolic quantum numbers, and  $R = \frac{(-2E)^{3/2}}{F}$ , where  $E$  is the energy and  $F$  the applied electric field. The quantity  $E$

may be calculated using the perturbative methods found in Ref. [31].

In order to perform this calculation, we must be able to change the basis of our state vector from the  $|n, j, m_j, \ell\rangle$  basis to the parabolic  $|n, n_1, n_2, m\rangle$  basis. We do this by first casting our wave function to the spherical  $|n, \ell, m, m_s\rangle$  basis, and then converting from the spherical basis to the parabolic basis. To convert a state  $|n, j, m_j, \ell\rangle$  basis to the spherical basis, we introduce the projection operator [32]

$$|n, j, m_j, \ell\rangle = \sum_{m, m_s} |n, \ell, m, m_s\rangle \langle n, \ell, m, m_s | n, j, m_j, \ell\rangle, \quad (7.2)$$

where the sum is over  $m$  and  $m_s$  that satisfy

$$m_j = m + m_s \quad (7.3)$$

$$m_s = \pm \frac{1}{2}. \quad (7.4)$$

The coefficients  $\langle n, \ell, m, m_s | n, j, m_j, \ell\rangle$  are Clebsch-Gordan coefficients, as introduced in Chapter 2.

To convert from the  $|n, \ell, m, m_s\rangle$  basis to the  $|n, n_1, n_2, m\rangle$  basis, we again introduce the projection operator [1]

$$|n, \ell, m, m_s\rangle = \sum_{n_1, n_2} |n, n_1, n_2, m\rangle \langle n, n_1, n_2, m | n, \ell, m, m_s\rangle, \quad (7.5)$$

where the sum is over nonnegative  $n_1$  and  $n_2$  such that

$$n_1 + n_2 = n - |m| - 1. \quad (7.6)$$

The coefficients  $\langle n, n_1, n_2, m | n, \ell, m, s, m_s \rangle$  are given by the equation

$$\langle n, n_1, n_2, m | n, \ell, m, m_s \rangle = \sqrt{\frac{2}{n}} (-1)^\ell P_{\ell, m} \left( \frac{n_1 - n_2}{n} \right). \quad (7.7)$$

With the change of basis now complete, we may calculate (7.1) and proceed with our treatment of ionization. It remains for us to implement these change of bases into our program, and to gain a better understanding of the calculation of the  $E$  term in (7.1), so that, too, may be implemented into our program.

## 7.2 Casting to a Quantum Control Experiment

Quantum control is an active area of research that seeks to govern the properties of a quantum mechanical system [33]. By “inverting” our algorithm, we could potentially create a quantum control experiment. To elaborate, currently, we submit a set of parameters to our algorithm and an ionization current is returned. To create a quantum control experiment, we must write a program that takes a desired ionization current and returns the parameters required to produce that current, thereby effectively controlling the energy state distribution of the atoms.

The potential to exhibit such control is easily seen in Figure 6.3; by choosing an appropriate delay time, we are able to control the size of the peaks seen in the ionization current. Of course, the parameter space extends well beyond the delay time. For instance, it also includes the details of the initial superposition and the shape of the ionization pulse as a function of time. A potential algorithm for exploring this parameter space is a genetic algorithm, though little substantial progress has been made toward this end [34].

With the equipment currently being used, the experimenters do not possess



precise control over the shape of the ionization pulse. However, there is the potential to use a new arbitrary waveform generator, which would give greater control over the shape of the pulse, but would not be able to produce a large enough field to ionize atoms in the  $46D_{5/2}$  state. Consequently, as a first step in the direction of creating a quantum control experiment, we plan to repeat the experiment done in this thesis at states of much higher  $n$  value, where the experimenters may both customize the shape of the ionization pulse, as well as create a large enough field to ionize the atoms.

# Bibliography

- [1] Thomas F. Gallagher. *Rydberg Atoms*. Number 3 in Cambridge Monographs on Atomic, Molecular, and Chemical Physics. Cambridge University Press, 1994.
- [2] W. R. Anderson, J. R. Veale, and T. F. Gallagher. Resonant dipole-dipole energy transfer in a nearly frozen rydberg gas. *Physical Review Letters*, 80:249–252, Jan 1998.
- [3] Immanuel Bloch, Jean Dalibard, and Wilhelm Zwerger. Many-body physics with ultracold gases. *Rev. Mod. Phys.*, 80:885–964, Jul 2008.
- [4] M. D. Lukin, M. Fleischhauer, R. Côté, L. M. Duan, D. Jaksch, J. I. Cirac, and P. Zoller. Dipole blockade and quantum information processing in mesoscopic atomic ensembles. *Phys. Rev. Lett.*, 87:037901, 2001.
- [5] Donald P. Fahey. *Resonant Dipole-Dipole Energy Transfer Dynamics in a Frozen Rydberg Gas*. PhD thesis, Bryn Mawr College, 2014.
- [6] Jesús V. Hernández. *Many-Body Dipole Interactions*. PhD thesis, Auburn University, 2008.
- [7] Michael A. Nielsen and Isaac L. Chuang. *Quantum Computation and Quantum Information*. Cambridge Series on Information and the Natural Sciences. Cambridge University Press, 10th edition, 2010.

- [8] D. Jaksch, J. I. Cirac, P. Zoller, S. L. Rolston, R. Côté, and M. D. Lukin. Fast quantum gates for neutral atoms. *Phys. Rev. Lett.*, 85(10):2208–2211, Sep. 2000.
- [9] T. G. Walker M. Saffman and K. Mølmer. Quantum information with rydberg atoms. *Review of Modern Physics*, 82:2313–236, 2010.
- [10] Kelly Cooper Younge. *Rydberg Atoms for Quantum Information*. PhD thesis, University of Michigan, 2010.
- [11] H. J. Metcalf and P. van der Straten. Laser cooling and trapping of atoms. *J. Opt. Soc. Am. B*, 20(5):887–908, May 2003.
- [12] Donald P. Fahey and Michael W. Noel. Excitation of rydberg states in rubidium with near infrared diode lasers. *Opt. Express*, 19(18):17002–17012, Aug 2011.
- [13] Jan R. Rubbmark, Michael M. Kash, Michael G. Littman, and Daniel Kleppner. Dynamical effects at avoided level crossings: A study of the landau-zener effect using rydberg atoms. *Phys. Rev. A*, 23:3107–3117, Jun 1981.
- [14] Weng Cho Chew. Quantum mechanics made simple: Lecture notes, Oct 2012.
- [15] Myron L. Zimmerman, Michael G. Littman, Michael M. Kash, and Daniel Kleppner. Stark structure of the rydberg states of alkali-metal atoms. *Phys. Rev. A*, 20:2251–2275, Dec 1979.
- [16] Wenhui Li, I. Mourachko, M. W. Noel, and T. F. Gallagher. Millimeter-wave spectroscopy of cold rb rydberg atoms in a magneto-optical trap: Quantum defects of the  $ns$ ,  $np$ , and  $nd$  series. *Phys. Rev. A*, 67:052502, May 2003.

- [17] Jianing Han, Yasir Jamil, D. V. L. Norum, Paul J. Tanner, and T. F. Gallagher. Rb  $nf$  quantum defects from millimeter-wave spectroscopy of cold  $^{85}\text{Rb}$  rydberg atoms. *Phys. Rev. A*, 74:054502, Nov 2006.
- [18] J. A. Petrus K. Afrousheh, P. Bohlouli-Zanjani and J. D. D. Martin. Determination of the  $^{85}\text{Rb}$   $ng$ -series quantum defect by electric-field induced resonant energy transfer between cold rydberg atoms. *Phys. Rev. A*, 74:062712, Dec 2006.
- [19] Mark Loewe Arno Bohm. *Quantum Mechanics: Foundations and Applications*, pages 165–172. Springer, 3 edition, 1993.
- [20] Edwin E. Salpeter Hans A. Bethe. *Quantum Mechanics of One and Two Electron Atoms*, page 7. Springer, 1977.
- [21] G. Wanner E. Hairer, S.P. Nørsett. *Solving Ordinary Differential Equations I Nonstiff Problems*, pages 462–464. Springer, 2 edition, 2008.
- [22] L. Landau. Zur theorie der energieubertragung. ii. *Physikalische Zeitschrift der Sowjetunion*, 2:46–51, 1932.
- [23] C. Zener. Non-adiabatic crossings of energy levels. *Proceedings of the Royal Society of London A*, 137(6):696–672, 1932.
- [24] C. Wesdorp F. Robicheaux and L. D. Noordam. Selective field ionization in li and rb: Theory and experiment. *Phys. Rev. A*, 62:043404, Sep. 2000.
- [25] B.T. Torosov and N.V. Vitanov. Evolution of superpositions of quantum states through a level crossing. *Phys. Rev. A*, 84:063411, Dec 2011.

- [26] S. S. Ivanov and N. V. Vitano. Steering quantum transitions between three crossing energy levels. *Phys. Rev. A*, 77:023406, Feb. 2008.
- [27] B.T. Torosov and N.V. Vitanov. NONADIABATIC TRANSITIONS DUE TO CURVE CROSSINGS: COMPLETE SOLUTIONS OF THE LANDAU-ZENER-STUECKELBERG PROBLEMS AND THEIR APPLICATIONS. *AIP Conference Proceedings*, 500:495–509, Feb 2000.
- [28] M. Førre and J.P. Hansen. Selective-field-ionization dynamics of a lithium  $m = 2$  rydberg state: Landau-zener model versus quantal approach. *Phys. Rev. A*, 67:053402, May 2003.
- [29] Ludwig Zehnder. Ein neuer interferenzrefraktor. *Zeitschrift fr Instrumentenkunde*, 11:275–285, 1891.
- [30] Ludwig Mach. Ueber einen interferenzrefraktor. *Zeitschrift fr Instrumentenkunde*, 12:89–93, 1892.
- [31] Harris J. Silverstone. Perturbation theory of the stark effect in hydrogen to arbitrarily high order. *Phys. Rev. A*, 18(5):1853–1864, Nov 1978.
- [32] John S. Townsend. *A Modern Approach to Quantum Mechanics*. University Science Books, 2000.
- [33] Claudio Altafini and Francesco Ticozzi. Modeling and control of quantum systems: An introduction. *IEEE Transactions on Automatic Control*, 57(8):1898–1917, 2012.
- [34] Stuart J. Russell and Peter Norvig. *Artificial Intelligence: A Modern Approach*, pages 126–129. Pearson Education, 2nd edition, 2003.

Advisor:

---

Dr. Thomas Carroll

Committee members:

---

Dr. Thomas Carroll

---

Dr. Douglas Nagy

---

Dr. Nicholas Scoville

Approved:

---

Dr. Douglas Nagy